energies

MDPI

Article

Model for Predicting CO_2 Adsorption in Coal Left in Goaf Based on Backpropagation Neural Network

Fei Gao [1,*], Peng Wang [1], Dapeng Wang [2], Yulong Yang [3], Xun Zhang [4] and Gang Bai [1]

[1] School of Safety Science and Engineering, Liaoning Technical University, Fuxin 123008, China
[2] Shanxi Jinshen Energy Co., Ltd., Xinzhou 034000, China
[3] Shanxi Hequ Jinshen Ciyaogou Coal Industry Co., Ltd., Xinzhou 036500, China
[4] College of Mining, Liaoning Technical University, Fuxin 123008, China
* Correspondence: gfgf2001@163.com; Tel.: +86-187-4184-6692

Abstract: Injecting power plant flue gas into a goaf stores CO_2 in the flue gas and effectively prevents the spontaneous combustion of the coal remaining in the goaf. Here, we investigated the adsorption behavior of three types of coal at normal temperature and pressure using a self-developed adsorption experimental device. We used a specific surface area and porosity analyzer to study the effects of pore structure, mineral content, and moisture content on CO_2 adsorption in coal. Based on the experimental data, we designed a multifactor CO_2 adsorption prediction model based on a backpropagation (BP) neural network. The results indicated that the pore size of most micropores in coal was in the range of 0.5–0.7 and 0.8–0.9 nm. The specific surface area and pore volume were positively correlated with the CO_2-saturated adsorption capacity, whereas the mean pore diameter, mineral content, and moisture content were inversely associated with the CO_2-saturated adsorption amount. The accuracy of the multifactor BP neural network prediction model was satisfactory: the determination coefficients (R^2) of the training and test sets were both above 0.98, the root mean square error (RMSE) and mean absolute error (MAE) of the test set were both less than 0.1, and the prediction results satisfied the requirements. To optimize the prediction performance of the model, we used the random forest algorithm to calculate the importance of each factor. The sum of the importance weights of the specific surface area, moisture content, and pore volume was 91.6%, which was much higher than that of the other two factors. Therefore, we constructed an optimization model with specific surface area, moisture content, and pore volume as input variables. The R^2 values of the training and test sets in the simplified model were improved compared with those of the multifactor model, the RMSE and MAE were reduced, and the fitting effect was ideal. The prediction model of CO_2 adsorption in coal based on the BP neural network can predict the CO_2 adsorption capacity of coal under different physical and chemical conditions, thereby providing theoretical support for the application of CO_2 storage technology in goafs.

Keywords: coal; pore structure; CO_2 sequestration; influence factors; machine learning

Citation: Gao, F.; Wang, P.; Wang, D.; Yang, Y.; Zhang, X.; Bai, G. Model for Predicting CO_2 Adsorption in Coal Left in Goaf Based on Backpropagation Neural Network. *Energies* **2023**, *16*, 3760. https://doi.org/10.3390/en16093760

Academic Editors: Dariusz Obracaj, Vasyl Lozynskyi and Ke Gao

Received: 29 March 2023
Revised: 24 April 2023
Accepted: 26 April 2023
Published: 27 April 2023

1. Introduction

In 2020, the Chinese government set the goals of carbon peaking by 2030 and carbon neutrality by 2060. Carbon capture and storage (CCS) is a technology used to collect and store CO_2 to reduce carbon emissions [1]. China has faced limitations in CCS development due to the high cost, large amounts of energy consumed for CO_2 capture, and high leakage risk posed by CO_2 storage [2–4]. Deng et al. [5] proposed injecting the flue gas of a power plant, with CO_2 as the main component, into goafs and storing CO_2 by using the CO_2-adsorption characteristics of the coal in goafs. This would not only reduce the expense of capturing and separating CO_2 from flue gas, but also effectively prevent the spontaneous combustion of coal left in the goaf, which is essential for the effective implementation of the national double carbon goals. However, the physical and chemical environments of

the goaf are challenging, and many factors affect the adsorption of CO_2 by coal seams. These include external factors such as pressure and temperature, as well as internal factors such as the coal pore structure, moisture, and minerals [6–9]. Chen et al. [10] studied the effect of CH_4 replacement with CO_2 in aquiferous coal and determined that as the moisture content increased, the adsorption capacity of coal for methane and carbon dioxide gradually weakened. Xie et al. [11] used MATLAB software to comprehensively discuss the influencing factors of CO_2 adsorption capacity of shale and determined that the total organic carbon (TOC) content was dominant, playing a major positive role. Quartz quality also had a positive impact. Abunowara et al. [12] reported that coal and rock exhibited temperature sensitivity to CO_2 adsorption, and their CO_2 adsorption capacity significantly decreased under high temperature conditions. Zhou et al. [13] analyzed the combined effects of temperature, particle size, and moisture content on CO_2 adsorption using a response surface model and discovered that particle size and moisture content had the strongest combined effect, followed by temperature and particle size, while temperature and moisture content had the weakest combined effect.

For many years, traditional adsorption models, including the Langmuir, D-A, D-R, and BET models, have been used to fit the experimental data of CO_2 adsorption [14–16]. Han et al. [17] conducted CO_2 isothermal adsorption experiments on coal and rock under different temperature conditions and established an improved evaluation model for coal seam CO_2 storage capacity. Although the traditional isothermal adsorption models can accurately explain the experimental data, these mechanism models are limited to specific temperatures, assumptions, and types of coal, and the experimental process is complex. Using existing adsorption data, Yu et al. [18] established a multiple linear regression equation of CO_2 adsorption amount and coal quality index parameters using SPSS software, and analyzed the influence of the coal quality index on CO_2 adsorption characteristics. In 2019, Meng et al. [19] proposed an innovative adsorption model based on a machine learning method that overcame the limitations imposed by coal type and could predict the adsorption behavior of coal according to basic coal physical and chemical parameters. Therefore, it is necessary to conduct research on prediction models for CO_2 adsorption capacity of coal, obtain the optimal conditions for CO_2 storage in goaf coal seams, and predict the CO_2 storage capacity under different physical and chemical conditions in goaf.

However, neither the traditional isothermal adsorption model nor the temperature–pressure comprehensive adsorption model can be used to analyze simultaneous changes in moisture content, pore structure, and mineral content [20]. In machine learning models, the prediction of the amount of CO_2 adsorbed by coal seams is a multiple regression problem [21]. With sufficient data, models based on machine learning can include all relevant variables. Therefore, in this study, we selected five influencing factors: specific surface area, pore volume, mean pore diameter, mineral content, and moisture content. We used a self-developed experimental device to perform CO_2 adsorption experiments with coal at normal temperature and pressure. Based on a large amount of experimental data, we designed a multifactor coupling influencing the CO_2 adsorption model based on a backpropagation (BP) neural network, and calculated the importance weight of each factor using a random forest algorithm to obtain the optimization model. The study results provide theoretical support for the application of CO_2 sequestration technology in goafs and are of practical value for reducing greenhouse gas emissions.

2. Materials and Methods

2.1. Coal Preparation

We extracted three types of coal samples, lignite, 1/3 coking coal, and gaseous coal, from the goaf of the Dananhu (DNH), Junde (JD), and Tongxin (TX) coal mines in Xinjiang, Heilongjiang, and Shanxi, respectively. The industrial and elemental analyses are shown in Table 1.

Table 1. Industrial analysis and elemental analysis of three coal samples.

Sample	Proximate Analysis w/%			Ultimate Analysis w/%				
	M_{ad}	A_{ad}	V_{daf}	C	H	O	N	S
DNH	12.02	15.08	38.28	88.53	3.03	6.58	1.13	0.73
JD	3.16	33.60	35.18	86.34	4.06	8.15	1.09	0.36
TX	0.80	20.85	32.53	80.89	4.67	13.14	0.82	0.48

We used a crusher to crush the raw coal to a particle size of <60 mesh (0.18 mm). In accordance with the national standard GB/T 7560-2001, we soaked the samples in aqueous HCl (5 mol/L) and HF (40%). After filtration, washing, and vacuum drying for 4 h, we obtained demineralized dry coal samples, which were marked as DNH-daf, JD-daf, and TX-daf and stored in a vacuum box.

To obtain dry coal samples with different mineral contents, we weighed six 200 g of DNH-daf, JD-daf, and TX-daf coal samples and subsequently added a certain amount of dry minerals with a particle size below 200 mesh (0.074 mm) [22]. We successively prepared coal samples with mineral contents of 0%, 3%, 6%, 9%, 12%, and 15%, which were labeled as DNH-M%, JD-M%, and TX-M%, where M% is the mineral content percentage. To simulate the actual mineral composition of coal [23], the mass ratio of each component in the mineral was m_{illite}:$m_{kaolinite}$:$m_{calcium\ carbonate}$:$m_{hematite}$:$m_{silica\ powder}$ = 2.5:22.5:1.7:0.7:2.6.

To produce demineralized coal samples with different moisture contents, we weighed seven 200 g DNH-daf, JD-daf, and TX-daf coal samples. We used a spray device to spray a certain amount of distilled water in the coal samples, which we then sealed and let stand for 12 h. The percentage of moisture quality and coal sample mass after water spraying was the actual moisture content of the coal sample. We successively prepared coal samples with water contents of 0%, 2%, 5%, 7%, 9%, 12%, and 15%, which were labeled as DNH-W%, JD-W%, and TX-W%, where W% is the moisture content.

2.2. Measurement of Pore Structure of Coal Samples

Micropores are the main adsorption pores of coal [24]. Therefore, we used an ASAP2020 specific surface area and porosity analyzer (Micromeritics Company, Norcross, GA, USA) to conduct isothermal adsorption experiments on the DNH-daf, JD-daf, and TX-daf coal samples using CO_2 as the probe. We used nonlocal density functional theory to calculate the micropore diameter (D), specific surface area (S), and pore volume (V) of the three coal samples. The results are presented in Table 2. It can be seen that DNH coal samples have the largest specific surface area and pore volume followed by JD coal, and TX coal has the smallest, while the average pore size is exactly the opposite.

Table 2. Pore structure parameters of three demineralized dry coal samples.

Sample No.	Pore Volume ($cm^3\ g^{-1}$)	Pore Diameter (nm)	Specific Surface Area ($m^2\ g^{-1}$)
DNH-daf	0.03851	0.568	132.38
JD-daf	0.02091	0.85	93.198
TX-daf	0.01544	0.97	75.843

2.3. Adsorption Experiment

We used a self-developed coal adsorption device in the adsorption experiment, as shown in Figure 1. To simulate the concentration of CO_2 in the flue gas of a power plant, the CO_2 concentration in the adsorbed gas was set to approximately 16%. To eliminate any interference from other gases in the flue gas, we used Ar as the mixed background gas.

Figure 1. CO_2 adsorption experimental system under normal temperature and pressure.

The experimental process involved placing the treated coal sample into the adsorption cylinder and degassing the adsorption cylinder using a vacuum pump after sealing to achieve a pressure of approximately −0.09 MPa. After degassing, we injected the experimental gas into the adsorption cylinder using a gas supply device; the pressure in the cylinder was slightly higher than 0.1 MPa. We determined the volume fraction of CO_2 in the cylinder every 30 min using a gas chromatograph, and we simultaneously recorded the pressure in the cylinder and ambient temperature for 6 h. Furthermore, we calculated the CO_2 content in the free phase of the cylinder before and after adsorption using the ideal gas state equation. The difference was the amount of CO_2 adsorbed by the coal sample, as shown in Equation (1).

$$V_i = \frac{(n_0 - n_i)V_m}{m} \times 10^3, \quad (1)$$

where V_i is the gas adsorption volume per gram of coal at a certain time point ($cm^3 \cdot g^{-1}$); V_m is the molar volume of gas under normal temperature (25 °C) and pressure, 24.5 L/mol; n_0 is the amount of CO_2 injected into the adsorption cylinder before adsorption (mol); n_i is the amount of CO_2 in the adsorption cylinder at the ith recording time (mol); and m is the mass of coal (g).

3. Results

3.1. Effect of Pore Structure on CO_2 Adsorption

Figure 2 shows the curve of the change in CO_2 adsorption capacity of the demineralized dry coal samples with time. We determined that the coal samples rapidly adsorbed CO_2 within the first hour at the beginning of adsorption, after which the CO_2 adsorption rate on the coal samples slowed and was stabilized after 4–6 h. We considered the average value of the adsorption amount during this period as the saturated adsorption amount Q of the coal samples for CO_2. The difference in CO_2-saturated adsorption capacity among the three coal samples was substantial. DNH coal had the highest saturated adsorption capacity, followed by JD and then TX coal. Because we demineralized and dried the coal samples, minerals and moisture had no influence on the adsorption of CO_2 by the coal. The difference in pore structure was the reason for the difference in saturated CO_2 adsorption.

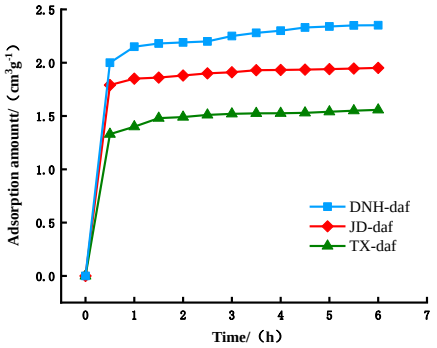

Figure 2. The adsorption capacity curve of demineralized dry coal samples.

Figure 3 shows the specific surface area, pore volume, and curve of the coal samples in the microporous range. In the figure, the cumulative specific surface area and pore volume curves of the three coal samples exhibit the same trend. The cumulative specific surface area and pore volume gradually increased with increasing pore size, indicating the presence of micropores <1 nm in the coal. The cumulative specific surface area and pore volume of DNH coal were the largest, followed by those of JD and TX coals, which was consistent with the order of the saturated CO_2 adsorption amount of the three coal samples.

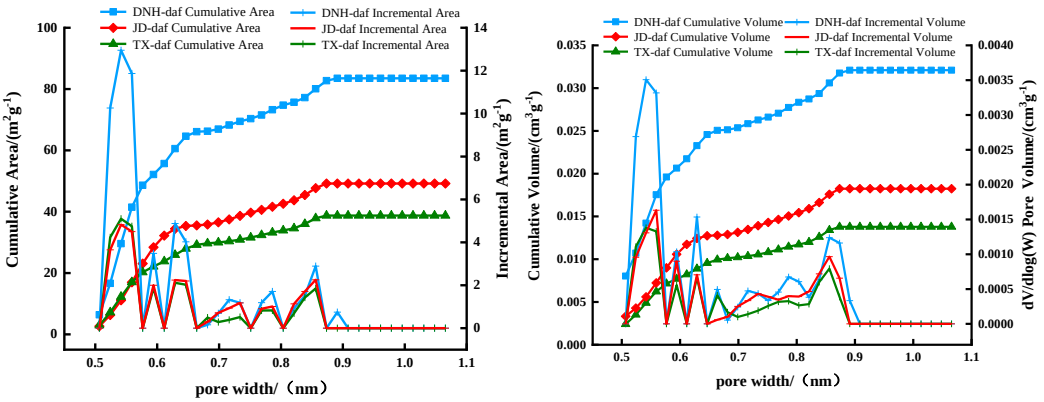

Figure 3. Specific surface area, pore volume and its increment curve of coal samples in microporous range. (**a**) Specific surface area and its increment curve. (**b**) Pore volume and its increment curve.

The curves of the specific surface area and pore volume increase in the coal samples reached maximum values in the pore diameter range of 0.5–0.7 and 0.8–0.9 nm, respectively, indicating the existence of many pores in these ranges. The curves of the specific surface area and pore volume increase reached their minimum values in the range of 0.7–0.8 nm, indicating that few pores were present in this size range. The pore size distribution laws of the three coal samples were similar, but the curves of the specific surface area and pore volume increase in DNH coal within the same pore size range were considerably higher than those of the other two coal samples. This was because DNH coal had more micropores within the same pore size range, which could provide more adsorption sites for CO_2 adsorption, resulting in its saturated adsorption capacity being higher than that of the other two coal samples.

To explore the influence of pore structure on the CO_2-saturated adsorption capacity, we plotted the relationship between the total specific surface area, total pore volume, and mean pore diameter of the coal samples measured in the experiment with CO_2-saturated adsorption, as shown in Figure 4. The specific surface area and pore volume of DNH coal sample are significantly higher than those of the other two coal samples, while the average pore size of TX coal sample is the largest, indicating that the micropores of DNH coal samples are more developed. The determination coefficient (R^2) of total specific surface area and CO_2-saturated adsorption capacity was the highest, at 0.955, indicating that the specific surface area was the main factor affecting CO_2-saturated adsorption capacity. Both the specific surface area and pore volume were positively correlated with the saturated adsorption capacity of CO_2 due to the larger total specific surface area and total pore volume of coal, which provided more adsorption sites and thus facilitated the adsorption of CO_2 by coal [25]. However, the mean pore diameter negatively correlated with the CO_2-saturated adsorption capacity. This may be because intermolecular forces were the main factor affecting the CO_2 adsorption effect. The smaller the pore diameter of each micropore, the higher the adsorption potential energy between the pore walls (due to the overlap of van der Waals force fields), and the higher the CO_2 adsorption capacity [26]. Additionally, the smaller the average pore diameter and the larger the number of micropores, the larger was the total specific surface area. As the specific surface area more strongly affected

the CO_2-saturated adsorption capacity, the saturated adsorption capacity of CO_2 by coal decreased with increasing pore diameter.

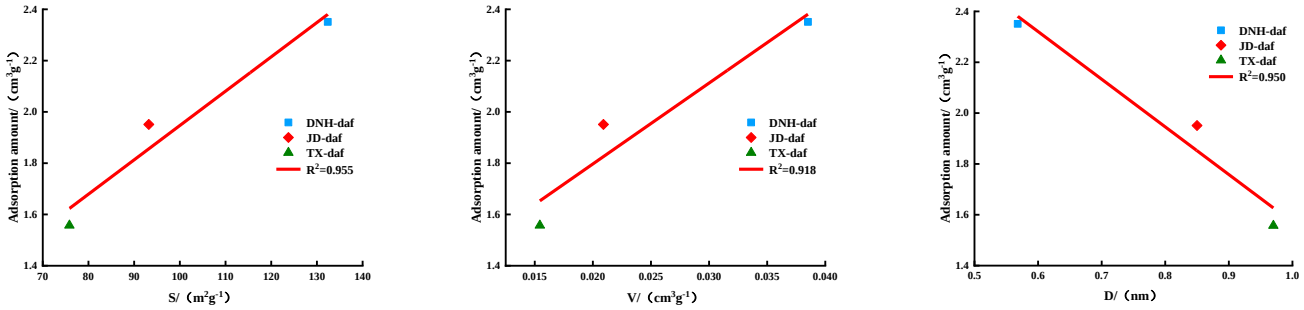

(**a**) Specific surface area (**b**) Pore volume (**c**) Pore diameter

Figure 4. Relationship between (**a**) specific surface area, (**b**) pore volume and (**c**) pore size and CO_2 saturated adsorption capacity.

3.2. Influence of Mineral Content on CO_2 Adsorption

Figure 5 shows the CO_2 adsorption curves of dry coal samples with different mineral contents. Similar to the demineralized dry coal samples, the variation in the CO_2 adsorption amount for each coal sample over time was consistent. With an increase in the mineral content, the CO_2 adsorption capacity of coal showed a decreasing trend because the minerals occupied the pore space in the coal, leading to a reduction in the number of coal adsorption sites and thus reducing the CO_2 adsorption capacity of coal. The CO_2 adsorption capacity of the three coal samples decreased with increasing mineral content to varying degrees, among which the saturated adsorption capacity of DNH coal decreased the most and that of TX coal decreased the least with increasing mineral content. This may have occurred because among the three coal samples with the same mineral contents, DNH coal had the largest number of micropores, which led to more minerals filling the micropores of coal in the form of bands and lumps [27]. Accordingly, we determined that the mineral content more strongly impacted the CO_2 adsorption capacity of DNH coal.

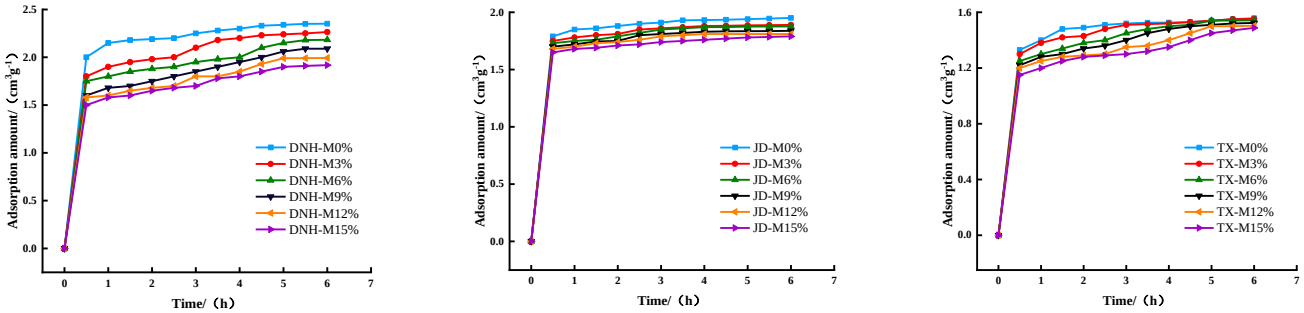

(**a**) Dananhu Formation (**b**) Junde Formation (**c**) Tongxin Formation

Figure 5. CO_2 adsorption curves of coal samples with different mineral contents.

3.3. Effect of Moisture Content on CO_2 Adsorption

Figure 6 shows the CO_2 adsorption curves of the coal samples with different moisture contents. When the water content was less than 9%, the CO_2-saturated adsorption capacity of the coal sample decreased with the increase in the moisture content. However, the saturated adsorption capacity of the three coal samples differed with the degree of water content reduction: the capacity of DNH coal was highest followed by those of JD coal and then TX coal. This occurred because the water molecules entered the coal body and occupied the pores [28]. The number of micropores in the DNH coal sample was the largest, leading to a higher reduction in the number of effective adsorption sites, and thus the adsorption capacity of DNH coal decreased. As the moisture content gradually increased, its influence on the adsorption capacity gradually decreased. When the moisture content

was higher than 9%, the adsorption curves of coal with different moisture contents tended to overlap. This occurred because with the increase in moisture content, water molecules gradually filled the cracks of coal, thereby blocking the diffusion channel of CO_2 molecules and preventing the entry of CO_2 molecules into the pores of the coal.

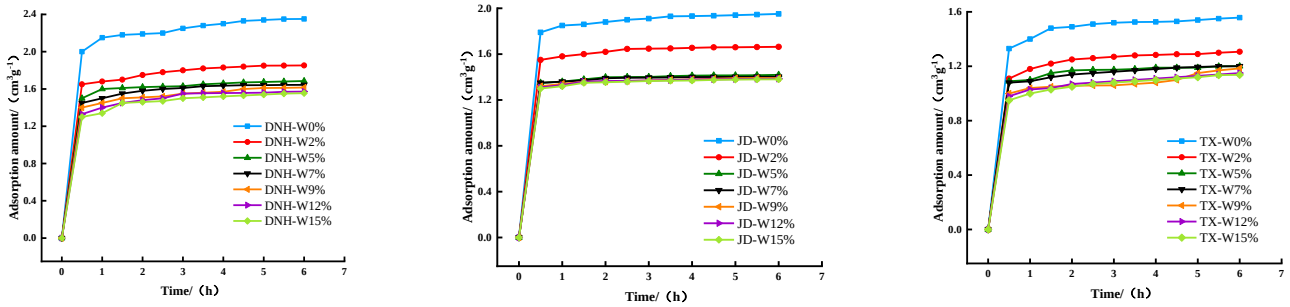

(**a**) Dananhu Formation (**b**) Junde Formation (**c**) Tongxin Formation

Figure 6. CO_2 adsorption curves of coal samples at different moisture contents.

4. BP Neural Network Prediction Model

4.1. Sample Data

Based on the previous experimental studies, we determined that the mean pore diameter, specific surface area, pore volume, moisture content, and mineral content affected CO_2 adsorption by coal. Therefore, to establish a model for predicting the CO_2-saturated adsorption capacity of goaf residual coal under the influence of multiple factors, we designed 126 groups of experiments using the control variable method to test the CO_2-saturated adsorption capacity of the three types of coal under various mineral and moisture contents. The experimental results are listed in Table A1; the statistical results for each variable in the experiment are presented in Table 3.

Table 3. The data of each characteristic parameter of the experiment.

Parameter	D (nm)	S (m^2 g^{-1})	V (cm^3 g^{-1})	W (%)	M (%)	Q (cm^3 g^{-1})
Average	0.726	117.282	0.0317	7.142	7.5	1.308
Maximum	0.87	132.38	0.038	15	15	2.351
Minimum	0.568	95.843	0.025	0	0	0.681
Variance	0.016	243.851	0.001	24.408	26.25	0.148

Owing to the large difference in the order of magnitude of each variable, the prediction model would have large errors. To ensure that the BP neural network would converge well and map the relationship, and to weaken the influence of data of different magnitudes for various factors on the network model training and prediction values, we used Equation (2) to normalize the experimental data. Subsequently, we converted all data of the training samples to the interval [0, 1].

$$X_{in} = \frac{X_i - X_{\min}}{X_{\max} - X_{\min}}, \quad (2)$$

where X_i is the independent variable in the sample data; $X_{\max}$ and $X_{\min}$ are the maximum and minimum values of the independent variables in the sample data, respectively; and X_{in} is the normalized independent variable.

4.2. Model Structure

A BP neural network is a multilayer feedforward network with forward signal transmission and back error transmission [29], which is applicable to scenarios where multiple structural characteristic parameters, complex influencing factors, and nonlinear relationships are being studied. The BP neural network comprises input, hidden, and output layers. The algorithm compares the expected output with the network output to obtain the error value, backpropagates the error value, modifies the weight value and threshold value layer

by layer until the error value reaches the preset error range, and completes the learning and memorization of information.

In this study, we selected five neurons in the input layer and one in the output layer. Increasing the number of hidden layer neurons can improve the mapping ability of BP neural networks, but when the number of neurons exceeds a certain value, the network performance deteriorates [30]. Therefore, the mean square error (MSE) and correlation coefficient® are generally used to determine the number of hidden layer neurons. Figure 7 shows the MSE and R values for different numbers of neurons.

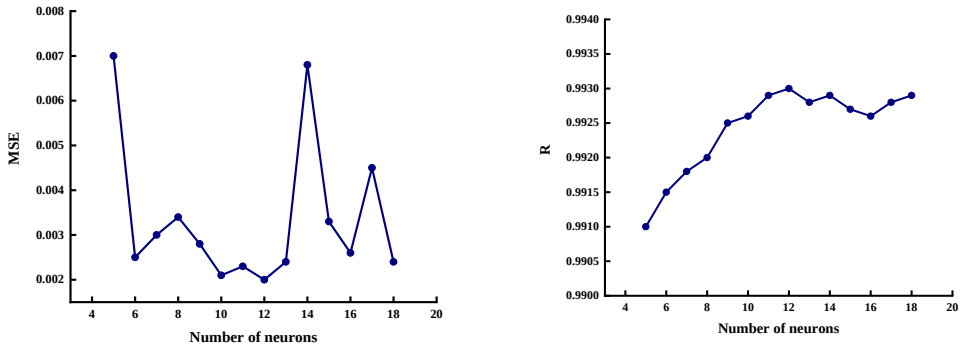

Figure 7. MSE and R values under different numbers of neurons.

Figure 7 shows that when the number of neurons was 12, the BP neural network performance was the best in terms of overall trend: the MSE was the lowest, the R value was the highest, the network convergence speed was faster, and the network was more stable. Therefore, we determined that the appropriate structure of the BP neural network was 5-12-1. We constructed a network structure, as shown in Figure 8, and used five factors (S, V, D, mineral content [M], and moisture content [W]) as the inputs of the BP neural network. Additionally, we used the saturated adsorption capacity of CO_2 (Q) as the output of the network.

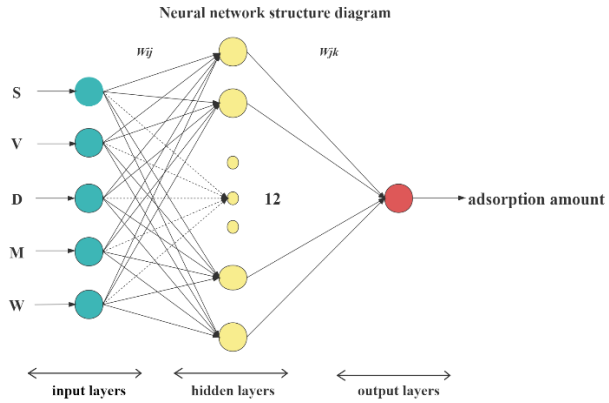

Figure 8. Structure diagram of BP neural network.

4.3. Model Training and Result Analysis

We randomly selected 80% (100 groups of data) of the experimental data as training samples, and used the remaining 20% (26 groups of data) as test samples. We continuously adjusted the learning rate as the number of iterations changes, determined the learning rate corresponding to the fastest decrease in loss, and ultimately set the initial learning rate to 0.4. In order to obtain the minimum value of the loss function, we set the minimum expected error to 0.0001, and the maximum number of iterations to 7000. Because the order of magnitude of the variables differed considerably, and the tanh function has the best effect when the features are remarkably different, we used tanh as the excitation function between the input and hidden layers. To maintain the numerical scaling of any previous

range and facilitate comparison with the sample values, we used purelin as the activation function between the hidden and output layers [31].

$$C(M,W,V,D,S) = \sum_{i=1}^{12} w_{6,i} \frac{e^{w_{1,i}*M+w_{2,i}*W+w_{3,i}*V+w_{4,i}*D+w_{5,i}*S+b_i} - e^{-(w_{1,i}*M+w_{2,i}*W+w_{3,i}*V+w_{4,i}*D+w_{5,i}*S+b_i)}}{e^{w_{1,i}*M+w_{2,i}*W+w_{3,i}*V+w_{4,i}*D+w_{5,i}*S+b_i} + e^{-(w_{1,i}*M+w_{2,i}*W+w_{3,i}*V+w_{4,i}*D+w_{5,i}*S+b_i)}} + b_0, \quad (3)$$

where M is the mineral content, %; W is the moisture content, %; V is the pore volume, $cm^3\ g^{-1}$; D is the mean pore diameter, nm; S is the specific surface area, $m^2\ g^{-1}$; $w_{1,i}$, $w_{2,i}$, $w_{3,i}$, $w_{4,i}$, and $w_{5,i}$ are the connection weights of each neuron from the input layer to the hidden layer; $w_{6,i}$ is the connection weight of each neuron from the hidden layer to the output layer; b_i is the bias between the neurons in the input and hidden layers; b_0 is the bias between the hidden- and output-layer neurons. Table 4 shows the optimal fitting results for all parameters.

Table 4. Optimal fitting parameters of BP neural network.

i	$w_{1,i}$	$w_{2,i}$	$w_{3,i}$	$w_{4,i}$	$w_{5,i}$	$w_{6,i}$	b_i	b_0
1	−0.065	−0.004	−0.193	0.086	−0.608	0.104	0.065	0.412
2	−0.108	−0.759	−0.481	0.188	0.151	−0.038	−0.644	
3	0.448	−0.523	0.175	0.48	0.263	−0.087	0.232	
4	−0.005	−0.556	0.209	−0.009	0.188	−0.102	−1.13	
5	0.248	0.181	0.243	−0.214	0.321	−0.042	0.245	
6	−0.104	0.009	0.018	0.113	−0.1	0.006	−0.045	
7	−0.36	−0.506	0.189	−0.499	−0.349	0.628	0.752	
8	−0.057	0.017	0.44	0.536	0.038	−0.369	−1.128	
9	0.203	0.317	0.093	0.174	0.406	−0.05	−0.245	
10	−0.049	−0.325	0.541	0.263	−0.388	−0.302	0.213	
11	−0.248	0.551	−0.094	−0.144	−0.145	0.369	0.267	
12	0.004	−0.429	−0.262	−0.376	0.324	0.802	0.996	

Figure 9 shows a joint scatter plot of the predicted CO_2-saturated adsorption amount calculated using the BP neural network model and the experimental value. In the figure, the x-axis represents the actual adsorption amount measured in the experiment, and the y-axis represents the adsorption amount predicted by the neural network. The black dotted line represents the 100% regression line. The closer the scatter is to the black dotted line, the more accurate the prediction of the neural network algorithm. Figure 8 shows that the data points of the training and test sets are distributed near the regression line, indicating that the trained model had high prediction accuracy.

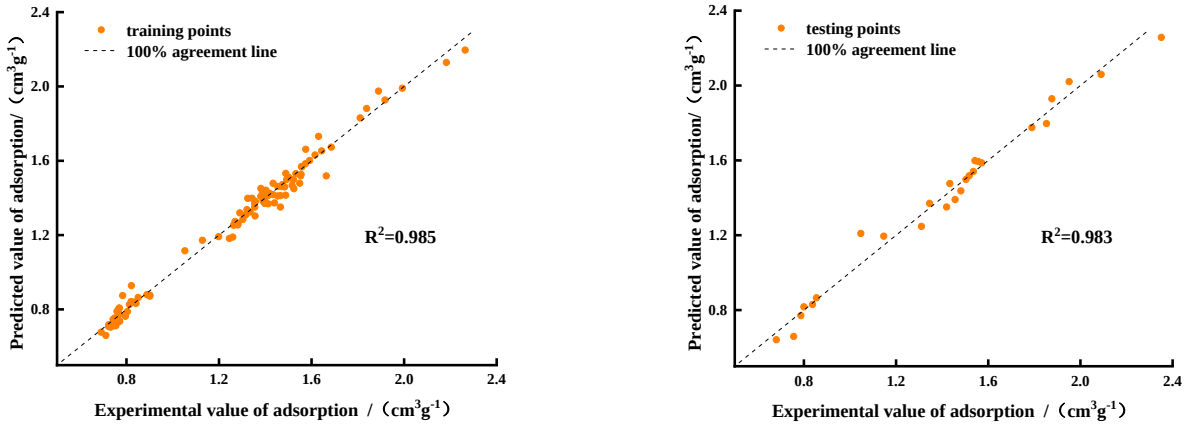

Figure 9. Performance of BP neural network training set and test set.

We evaluated the model to verify its accuracy. From a statistical point of view, we could not use a single performance index for the evaluation. Therefore, we selected three performance indicators, namely determination coefficient (R^2), root mean square

error (*RMSE*), and mean absolute error (*MAE*) to comprehensively evaluate the model. The calculation methods are shown in Equations (4)–(6), respectively.

$$R^2 = 1 - \frac{\sum(\hat{y}_i - y_i)^2}{\sum(y_i - \bar{y}_i)^2}, \tag{4}$$

$$RMSE = \sqrt{\frac{1}{n}\sum_{i=1}^{n}(y_i - \hat{y}_i)^2}, \tag{5}$$

$$MAE = \frac{1}{n}\sum_{i=1}^{n}|\hat{y}_i - y_i|, \tag{6}$$

where $\hat{y}_i$, y_i, and $\bar{y}_i$ are the predicted, actual, and average values of the target characteristics, respectively; and n is the total number of data.

Table 5 presents the results of the evaluation indices. The R^2 of the model for the training and test data was 0.985 and 0.983, respectively, which proved that the proposed adsorption model could accurately predict the saturated CO_2 adsorption amount from coal seams in the goaf under multifactor conditions. The R^2 difference between the training and test set was 0.002, which is small, indicating that the model was not overfit and had a certain generalization ability. Overfitting means that the model accurately reflects the noise and random fluctuation in the training data, but performs poorly in the test set, thus reducing the generalizability of the model [32]. In the test set, the RMSE and MAE were 0.055 and 0.045, respectively, which are both less than 0.1, indicating that the dispersion and deviation between the real and predicted values were small. The prediction results satisfy the requirements for predicting the saturated CO_2 adsorption by coal.

Table 5. Evaluation indexes of BP neural network model.

	Training Set	**Testing Set**
R^2	0.985	0.983
RMSE	0.044	0.055
MAE	0.033	0.045

5. Optimization Model

According to Equation (3), the model could predict the CO_2-saturated adsorption capacity of coal samples with certain mineral and moisture contents, mean pore diameter, pore volume, and specific surface area. However, Equation (3) is complex with too many input parameters, and researchers may not always be able to provide all these basic parameters. Predicting the CO_2-saturated adsorption capacity with fewer parameters would be more practical and helpful, and could improve the performance of the prediction model. To explore the importance of various factors on CO_2 adsorption by coal, we used scikit-learn with a random forest algorithm to calculate the importance of each feature [33]. Scikit-learn automatically calculates the score of each feature after training and then normalizes the results so that the sum of the importance of all features equals one. Figure 9 shows the calculated results for the importance of mineral content, moisture content, mean pore diameter, pore volume, and specific surface area.

Figure 10 shows the overall influence of the five input characteristics on the target variable. The specific surface area was the most influential factor among the five factors, and water content was more influential than pore volume. Moreover, the sum of the importance weights of the specific surface area, moisture content, and hole volume was 91.6%, which was much higher than those of the other two factors. However, the mean pore diameter and mineral content had little effect on the adsorption capacity.

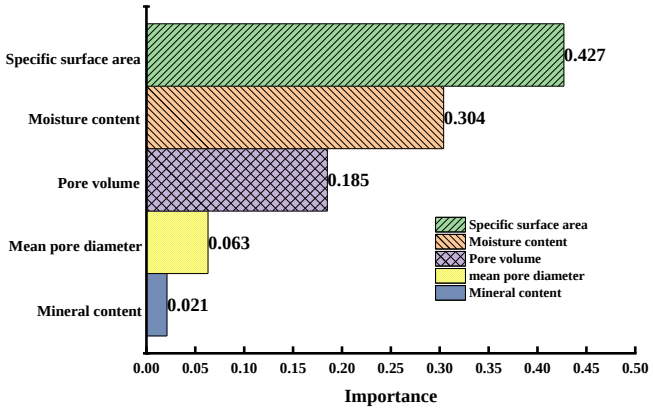

Figure 10. Importance weight of each factor.

Based on the above analysis and to simplify the input parameters of the model, we used the specific surface area, moisture content, and pore volume as the input units, and the BP neural network model parameter settings were the same as above. We established the functional expression of CO_2-saturated adsorption capacity as the output unit as follows:

$$C(S,W,V) = \sum_{i=1}^{12} w_{4,i} \frac{e^{w_{1,i}*S+w_{2,i}*W+w_{3,i}*V+b_i} - e^{-(w_{1,i}*S+w_{2,i}*W+w_{3,i}*V+b_i)}}{e^{w_{1,i}*S+w_{2,i}*W+w_{3,i}*V+b_i} + e^{-(w_{1,i}*S+w_{2,i}*W+w_{3,i}*V+b_i)}} + b_0. \quad (7)$$

The optimal fitting results of all parameters are shown in Table 6.

Table 6. Optimal fitting parameters of optimization model.

i	$w_{1,i}$	$w_{2,i}$	$w_{3,i}$	$w_{4,i}$	b_i	b_0
1	0.5	0.051	0.241	0.459	0.477	0.712
2	0.017	0.471	−0.413	−0.321	0.992	
3	−0.184	−0.588	0.021	0.284	−0.565	
4	0.248	0.247	0.458	0.247	−0.309	
5	0.071	2.165	0.005	−2.625	3.234	
6	−0.452	0.195	−0.17	0.401	0.543	
7	1.434	0.185	−0.091	1.083	0.856	
8	0.194	1.481	−0.141	1.142	1.607	
9	−0.035	0.015	−0.138	0.046	0.051	
10	−0.332	−0.491	−0.133	0.222	−0.418	
11	0.32	0.104	−0.027	0.486	0.494	
12	0.186	0.732	−0.001	−0.455	0.735	

Figure 11 shows that the data points of the three-variable model are distributed near the regression line; the R^2 of the training set was 0.991 and that of the test set was 0.988, which also showed that the model prediction accuracy was high. Compared with the multifactor prediction model (3), the prediction results of the simplified model (7) were closer to the verified data. To test the accuracy of the simplified model, we compared the real and predicted values of the training and test sets, and we calculated the evaluation indicators, which are listed in Table 7.

Table 7 shows that the RMSE and MAE of model (7) were lower than those of Model (3) by 0.6% and 1.5%, respectively. The RMSE and MAE on the test set were lower by 0.1% and 1.6%, respectively, and the fitting effect was more ideal. The simplified model not only provides more accurate prediction results, but also has a more direct expression. The proposed CO_2 saturation adsorption prediction model breaks the limitation of coal types. By measuring the basic parameters of coal samples from different goaf areas, the adsorption capacity of CO_2 by coal can be predicted.

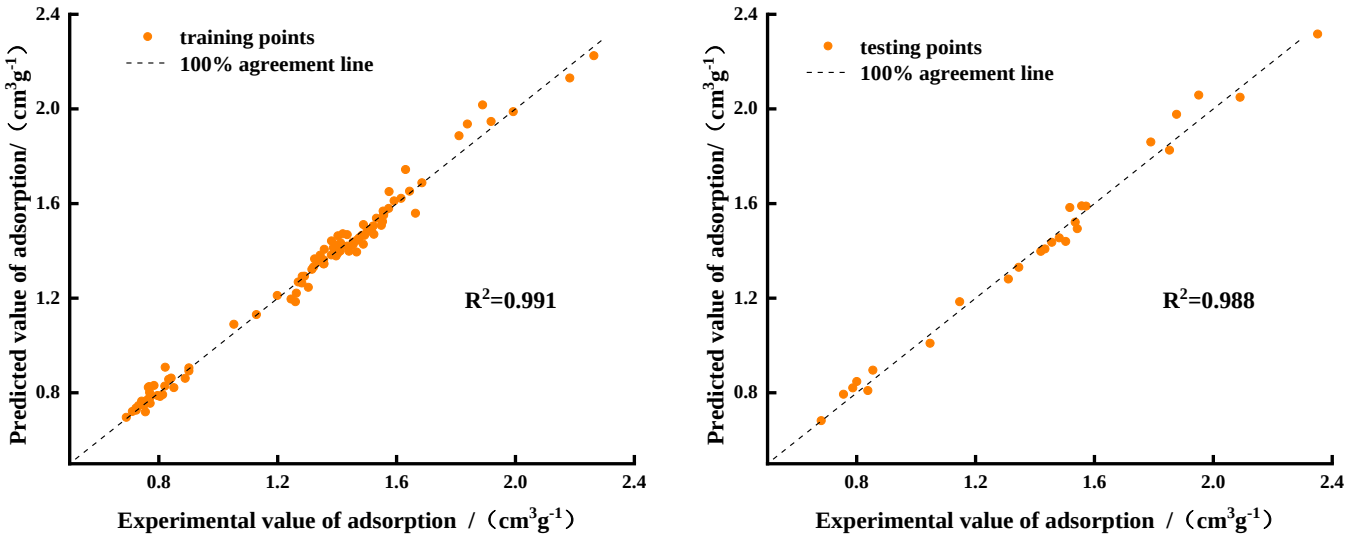

Figure 11. Performance of optimized BP neural network model training and testing sets.

Table 7. Evaluation indexes of optimized BP neural network model.

	Training Set	Testing Set
R^2	0.991	0.988
RMSE	0.038	0.040
MAE	0.032	0.029

6. Conclusions

The article analyzes the effects of pore structure, mineral content, and water content on the adsorption of CO_2 by coal based on a large amount of experiment, and a multi-factor CO_2 adsorption prediction model based on BP neural network is proposed, which is of great significance for evaluating the capacity of CO_2 storage in abandoned coal mines. The conclusions are summarized as follows:

(1) The pore size distributions of the three coal samples were largely similar, DNH coal had the most micropores in each pore size range, and TX coal had the fewest. The CO_2-saturated adsorption capacity of coal was positively correlated with the specific surface area and pore volume, and negatively correlated with the mean pore diameter, mineral content, and moisture content. When the moisture content was higher than 9%, the influence of water content on the saturated adsorption tended to be stable because water molecules hindered the CO_2 diffusion channels.

(2) The BP neural network prediction model with mineral content, moisture content, mean pore diameter, pore volume, and specific surface area as input variables had high accuracy: the R^2 values on the training and test sets were both higher than 0.98, and the RMSE and MAE on the test set were both less than 0.1. The prediction results met the expected requirements.

(3) To optimize the prediction performance of the model, we used a random forest algorithm to calculate the importance of each factor. We determined that the sum of the importance weights of the specific surface area, moisture content, and pore volume was 91.6%, which was much higher than that of the other two factors. Therefore, we constructed a simplified model with the specific surface area, moisture content, and pore volume as the input variables. Compared with the multifactor model, the R^2 of the training and test sets of the simplified model was higher, whereas the RMSE and MAE were lower, and the fitting effect was more accurate.

Author Contributions: F.G.: Supervision, Resources, Writing—review and editing, Validation; P.W.: Conceptualization, Methodology, Writing—original draft; D.W.: Project administration, Data curation; Y.Y.: Funding acquisition; X.Z.: Software; G.B.: Visualization. All authors have read and agreed to the published version of the manuscript.

Funding: This work was financially supported by the National Natural Science Foundation of China (51874161, 52074147, 52274204).

Data Availability Statement: The [CO_2 adsorption capacity] data used to support the results of this study is included in Appendix A; The remaining data used to support the findings of this study are available from the corresponding author upon request.

Conflicts of Interest: The authors declare that they have no known competing financial interests or personal relationships that could have appeared to influence the work reported in this paper.

Appendix A

Table A1. Test results of control variable method.

No.	Mineral Content (%)	Moisture Content (%)	Pore Volume ($cm^3\ g^{-1}$)	Pore Width (nm)	Specific Surface Area ($m^2\ g^{-1}$)	Adsorption Amount ($cm^3\ g^{-1}$)
1	0	0	0.03851	0.568	132.38	2.351122912
2	3	0	0.03851	0.568	132.38	2.263786921
3	6	0	0.03851	0.568	132.38	2.182949968
4	9	0	0.03851	0.568	132.38	2.090050028
5	12	0	0.03851	0.568	132.38	1.992612003
6	15	0	0.03851	0.568	132.38	1.917846123
7	0	2	0.03851	0.568	132.38	1.85279631
8	0	5	0.03851	0.568	132.38	1.685271318
9	0	7	0.03851	0.568	132.38	1.643701437
10	0	9	0.03851	0.568	132.38	1.615139692
11	0	12	0.03851	0.568	132.38	1.571735379
12	0	15	0.03851	0.568	132.38	1.55467822
13	3	2	0.03851	0.568	132.38	1.630202661
14	3	5	0.03851	0.568	132.38	1.591743463
15	3	7	0.03851	0.568	132.38	1.573359782
16	3	9	0.03851	0.568	132.38	1.556722672
17	3	12	0.03851	0.568	132.38	1.535297912
18	3	15	0.03851	0.568	132.38	1.521458693
19	6	2	0.03851	0.568	132.38	1.575013315
20	6	5	0.03851	0.568	132.38	1.532489236
21	6	7	0.03851	0.568	132.38	1.517203444
22	6	9	0.03851	0.568	132.38	1.501267535
23	6	12	0.03851	0.568	132.38	1.492639572
24	6	15	0.03851	0.568	132.38	1.474250565
25	9	2	0.03851	0.568	132.38	1.556956357
26	9	5	0.03851	0.568	132.38	1.51609469
27	9	7	0.03851	0.568	132.38	1.483624762
28	9	9	0.03851	0.568	132.38	1.471496057
29	9	12	0.03851	0.568	132.38	1.453800003
30	9	15	0.03851	0.568	132.38	1.433440237
31	12	2	0.03851	0.568	132.38	1.488459061
32	12	5	0.03851	0.568	132.38	1.466026662
33	12	7	0.03851	0.568	132.38	1.454078559
34	12	9	0.03851	0.568	132.38	1.433651718
35	12	12	0.03851	0.568	132.38	1.410745839
36	12	15	0.03851	0.568	132.38	1.401701778
37	15	2	0.03851	0.568	132.38	1.434080668
38	15	5	0.03851	0.568	132.38	1.412549898
39	15	7	0.03851	0.568	132.38	1.397531683
40	15	9	0.03851	0.568	132.38	1.356791458
41	15	12	0.03851	0.568	132.38	1.342959591
42	15	15	0.03851	0.568	132.38	1.324337967
43	0	0	0.02091	0.85	93.198	1.951122912
44	3	0	0.02091	0.85	93.198	1.889568493
45	6	0	0.02091	0.85	93.198	1.876259611
46	9	0	0.02091	0.85	93.198	1.838473984
47	12	0	0.02091	0.85	93.198	1.810181965

Table A1. *Cont.*

No.	Mineral Content (%)	Moisture Content (%)	Pore Volume ($cm^3\ g^{-1}$)	Pore Width (nm)	Specific Surface Area ($m^2\ g^{-1}$)	Adsorption Amount ($cm^3\ g^{-1}$)
48	15	0	0.02091	0.85	93.198	1.789616843
49	0	2	0.02091	0.85	93.198	1.66378542
50	0	5	0.02091	0.85	93.198	1.419339798
51	0	7	0.02091	0.85	93.198	1.402840159
52	0	9	0.02091	0.85	93.198	1.381119521
53	0	12	0.02091	0.85	93.198	1.395036416
54	0	15	0.02091	0.85	93.198	1.390437306
55	3	2	0.02091	0.85	93.198	1.548979178
56	3	5	0.02091	0.85	93.198	1.456424261
57	3	7	0.02091	0.85	93.198	1.411376369
58	3	9	0.02091	0.85	93.198	1.387666795
59	3	12	0.02091	0.85	93.198	1.380848091
60	3	15	0.02091	0.85	93.198	1.35472688
61	6	2	0.02091	0.85	93.198	1.481463143
62	6	5	0.02091	0.85	93.198	1.465782153
63	6	7	0.02091	0.85	93.198	1.440040993
64	6	9	0.02091	0.85	93.198	1.396502878
65	6	12	0.02091	0.85	93.198	1.354245284
66	6	15	0.02091	0.85	93.198	1.31527864
67	9	2	0.02091	0.85	93.198	1.419456467
68	9	5	0.02091	0.85	93.198	1.356062195
69	9	7	0.02091	0.85	93.198	1.334571319
70	9	9	0.02091	0.85	93.198	1.321037039
71	9	12	0.02091	0.85	93.198	1.290009358
72	9	15	0.02091	0.85	93.198	1.28157462
73	12	2	0.02091	0.85	93.198	1.34542688
74	12	5	0.02091	0.85	93.198	1.310368091
75	12	7	0.02091	0.85	93.198	1.282575827
76	12	9	0.02091	0.85	93.198	1.269113512
77	12	12	0.02091	0.85	93.198	1.262636166
78	12	15	0.02091	0.85	93.198	1.259852608
79	15	2	0.02091	0.85	93.198	1.30294852
80	15	5	0.02091	0.85	93.198	1.24487263
81	15	7	0.02091	0.85	93.198	1.198464723
82	15	9	0.02091	0.85	93.198	1.146836779
83	15	12	0.02091	0.85	93.198	1.12854191
84	15	15	0.02091	0.85	93.198	1.052667414
85	0	0	0.01544	0.97	75.843	1.557429647
86	3	0	0.01544	0.97	75.843	1.552752651
87	6	0	0.01544	0.97	75.843	1.542438976
88	9	0	0.01544	0.97	75.843	1.523701004
89	12	0	0.01544	0.97	75.843	1.503427565
90	15	0	0.01544	0.97	75.843	1.48793197
91	0	2	0.01544	0.97	75.843	1.047077437
92	0	5	0.01544	0.97	75.843	0.901155248
93	0	7	0.01544	0.97	75.843	0.901154164
94	0	9	0.01544	0.97	75.843	0.888796492
95	0	12	0.01544	0.97	75.843	0.850413237
96	0	15	0.01544	0.97	75.843	0.837536417
97	3	2	0.01544	0.97	75.843	0.854357295
98	3	5	0.01544	0.97	75.843	0.841515153
99	3	7	0.01544	0.97	75.843	0.83332657
100	3	9	0.01544	0.97	75.843	0.820373017
101	3	12	0.01544	0.97	75.843	0.812911451
102	3	15	0.01544	0.97	75.843	0.80442598
103	6	2	0.01544	0.97	75.843	0.82152556
104	6	5	0.01544	0.97	75.843	0.76488891
105	6	7	0.01544	0.97	75.843	0.767667102
106	6	9	0.01544	0.97	75.843	0.769085643
107	6	12	0.01544	0.97	75.843	0.759046084
108	6	15	0.01544	0.97	75.843	0.74239855
109	9	2	0.01544	0.97	75.843	0.80019876
110	9	5	0.01544	0.97	75.843	0.795644082
111	9	7	0.01544	0.97	75.843	0.786988804
112	9	9	0.01544	0.97	75.843	0.769035918
113	9	12	0.01544	0.97	75.843	0.750216039
114	9	15	0.01544	0.97	75.843	0.731744114

Table A1. *Cont.*

No.	Mineral Content (%)	Moisture Content (%)	Pore Volume ($cm^3\ g^{-1}$)	Pore Width (nm)	Specific Surface Area ($m^2\ g^{-1}$)	Adsorption Amount ($cm^3\ g^{-1}$)
115	12	2	0.01544	0.97	75.843	0.783710237
116	12	5	0.01544	0.97	75.843	0.770930791
117	12	7	0.01544	0.97	75.843	0.768939099
118	12	9	0.01544	0.97	75.843	0.758702093
119	12	12	0.01544	0.97	75.843	0.724040182
120	12	15	0.01544	0.97	75.843	0.711191055
121	15	2	0.01544	0.97	75.843	0.755654242
122	15	5	0.01544	0.97	75.843	0.754867438
123	15	7	0.01544	0.97	75.843	0.749298693
124	15	9	0.01544	0.97	75.843	0.723388924
125	15	12	0.01544	0.97	75.843	0.690732757
126	15	15	0.01544	0.97	75.843	0.680732757

References

1. Pigeon, J. What Carbon Capture and Storage (CCS) is Expected to? Describing Potential Future of a CO_2 Mitigation Technological System in the Seine Waterway Axis. *Energy Procedia* **2017**, *114*, 7333–7342. [CrossRef]
2. Zeng, R.S.; Vincent, C.J.; Tian, X.Y.; Stephenson, M.H.; Wang, S.; Xu, W.D. New potential carbon emission reduction enterprises in China: Deep geological storage of CO_2 emitted through industrial usage of coal in China. *Greenh. Gases Sci. Technol.* **2013**, *3*, 106–115. [CrossRef]
3. Minchener, A.J. Gasification based CCS challenges and opportunities for China. *Fuel* **2014**, *116*, 904–909. [CrossRef]
4. Zhang, X.; Fan, J.L.; Wei, Y.M. Technology roadmap study on carbon capture, utilization and storage in China. *Energy Policy* **2013**, *59*, 536–550. [CrossRef]
5. Gao, F.; Deng, C.B.; Wang, X.F.; Wu, S.W. Analysis on feasibility and safety in sealing of smoke injected into goaf. *J. Saf. Sci. Technol.* **2016**, *12*, 60–64.
6. Qu, S.J.; Yang, J.L.; Liu, Z.Y. CO_2 Sorption on Coals: Contribution of Minerals and Influence of Supercritical CO_2 Pre-exposure. *Energy Fuels* **2012**, *26*, 3928–3934. [CrossRef]
7. Wang, X.F.; Deng, C.B.; Qiao, L.; Chu, G.; Jing, R.; Kang, Y.L. A study on factors influencing CO_2 adsorption by coal. *AIP Adv.* **2021**, *11*, 035238. [CrossRef]
8. Guan, C.; Liu, S.M.; Li, C.W.; Wang, Y.; Zhao, Y.X. The temperature effect on the methane and CO_2 adsorption capacities of Illinois coal. *Fuel* **2018**, *211*, 241–250. [CrossRef]
9. Zhu, H.Q.; Guo, S.; Xie, Y.Y.; Zhao, H.R. Molecular simulation and experimental studies on CO_2 and N_2 adsorption to bituminous coal. *Environ. Sci. Pollut. Res.* **2021**, *28*, 15673–15686. [CrossRef]
10. Chen, L.; Zhao, M.; Li, X.; Liu, Y. Impact research of CH_4 replacement with CO_2 in hydrous coal under high pressure injection. *Min. Miner. Depos.* **2022**, *16*, 121–126. [CrossRef]
11. Xie, W.D.; Wang, M.; Dai, X.G. CO_2 adsorption characteristics and its affecting factors of lower Silurian, Longmaxi formation shale in southeast Chongqing. *J. Henan Polytech. Univ. (Nat. Sci.)* **2018**, *37*, 80–88.
12. Abunowara, M.; Sufian, S.; Bustam, M.A. Experimental measurements of carbon dioxide, methane and nitrogen high-pressure adsorption properties onto Malaysian coals under various conditions. *Energy* **2020**, *210*. [CrossRef]
13. Zhou, X.H.; Niu, Y.P.; Bai, G.; Zhang, X.W. Experimental study on factors affecting volume of CO_2 adsorbed by coal. *China Saf. Sci. J.* **2019**, *29*, 85–90.
14. Zhang, R.; Liu, S.M. Experimental and theoretical characterization of methane and CO_2 sorption hysteresis in coals based on Langmuir desorption. *Int. J. Coal Geol.* **2017**, *171*, 49–60. [CrossRef]
15. Zhou, J.P.; Liu, M.H.; Xian, X.F.; Jiang, Y.D.; Liu, Q.L.; Wang, X.C. Measurements and modelling of CH4 and CO_2 adsorption behaviors on shales: Implication for CO_2 enhanced shale gas recovery. *Fuel* **2019**, *251*, 293–306. [CrossRef]
16. Gao, T.; Deng, C.B.; Han, Q. Experimental Research on the Law of Energy Conversion during CO_2 Sequestration in Coal. *Energies* **2021**, *14*, 8079. [CrossRef]
17. Han, S.; Sang, S.; Zhang, J.; Xiang, W.; Xu, A. Assessment of CO_2 geological storage capacity based on adsorption isothermal experiments at various temperatures: A case study of No. 3 coal in the Qinshui Basin. *Petroleum* 2022, *in press*. [CrossRef]
18. Yu, H.G.; Fan, W.T.; Sun, M.Y.; Ye, J.P. Characteristi cs and prediction for adsorption iso-therms of carbon dioxide binary gas on coals. *J. China Coal Soc.* **2005**, *30*, 618.
19. Meng, M.; Qiu, Z.S.; Zhong, R.Z.; Liu, Z.G.; Liu, Y.F.; Chen, P.J. Adsorption characteristics of supercritical CO_2/CH_4 on different types of coal and a machine learning approach. *Chem. Eng. J.* **2019**, *368*, 847–864. [CrossRef]
20. Zhong, L.W.; Zheng, Y.Z.; Yuan, Z.R.; Lei, C.L.; Zhang, H. Adsorption performance of coal under the combined influence of temperature and pressure and prediction of gas content. *J. Coal Ind.* **2002**, *6*, 581–585.
21. Chattaraj, S.; Mohanty, D.; Kumar, T.; Halder, G.; Mishra, K. Comparative study on sorption characteristics of coal seams from Barakar and Raniganj formations of Damodar Valley Basin, India. *Int. J. Coal Geol.* **2019**, *212*, 103202. [CrossRef]

22. Li, M.Q.; Zhang, Z.X.; Wu, X.J.; Fan, J.J. Experiment and Mechanism Study on the Effect of Kaolin on Melting Characteristics of Zhundong Coal Ash. *Energy Fuels* **2016**, *30*, 7763–7769. [CrossRef]
23. Du, Q.H.; Liu, X.L.; Wang, E.Z.; Zuo, J.P.; Wang, W.M.; Zhu, Y.J. Effects of CO_2–water interaction with coal on mineral content and pore characteristics. *J. Rock Mech. Geotech. Eng.* **2020**, *12*, 326–337. [CrossRef]
24. Gao, F.; Xia, J.; Sun, R.J.; Shan, Y.F.; Jia, Z. Effects of inhibitors on the sequestration of flue gas in goaf and pore structures of coal. *Fuel* **2022**, *310*, 122354. [CrossRef]
25. Zhu, Y.M.; Wang, Y.; Chen, S.B.; Zhang, H.; Fu, C.Q. Qualitative-quantitative multiscale characterization of pore structures in shale reservoirs: A case study of longmaxi formation in the upper yangtze area. *Earth Sci. Front.* **2016**, *23*, 154–163. [CrossRef]
26. Liu, J.; Xie, H.; Wang, Q.; Chen, S.Y.; Hu, Z.M. The Effect of Pore Size on Shale Gas Recovery with CO_2 Sequestration: Insight into Molecular Mechanisms. *Energy Fuels* **2019**, *33*, 2897–2907. [CrossRef]
27. Fu, X.X.; Zhang, D.F.; Jiang, W.P.; Lun, J.Z.; Zhao, C.P.; Wang, H.T.; Li, Y.H. Influence of physicochemical properties of coals on pore morphology and methane adsorption:a perspective. *Chem. Ind. Eng. Prog.* **2019**, *38*, 2714–2725. [CrossRef]
28. Švábová, M.; Weishauptová, Z.; Přibyl, O. The effect of moisture on the sorption process of CO_2 on coal. *Fuel* **2012**, *92*, 187–196. [CrossRef]
29. Zhang, Y.Z. Application of improved BP neural network based on e-commerce supply chain network data in the forecast of aquatic product export volume. *Cogn. Syst. Res.* **2019**, *57*, 228–235. [CrossRef]
30. Jiang, Z.Y.; Gyurova, L.; Zhang, Z.; Friedrich, K.; Schlarb, A.K. Neural network based prediction on mechanical and wear properties of short fibers reinforced polyamide composites. *Mater. Des.* **2008**, *29*, 628–637. [CrossRef]
31. Li, B.Y.; Li, Y.X.; Wang, H.T.; Ma, Y.M.; Hu, Q.; Ge, F.L. Compensation of automatic weighing error of belt weigher based on BP neural network. *Measurement* **2018**, *129*, 625–632. [CrossRef]
32. Colaresi, M.; Mahmood, Z. Do the robot: Lessons from machine learning to improve conflict forecasting. *J. Peace Res.* **2017**, *54*, 193–214. [CrossRef]
33. Fan, W.; Liu, K.; Liu, H.; Wang, P.; Ge, Y.; Fu, Y. AutoFS: Automated Feature Selection via Diversity-Aware Interactive Reinforcement Learning. In Proceedings of the 2020 IEEE International Conference on Data Mining (ICDM), Sorrento, Italy, 17–20 November 2020; pp. 1008–1013. [CrossRef]